

A self-indicating cellulose-based gel with tunable performance for bioactive agent delivery

Abstract

Development of carriers with tunable properties can enhance the controllability of the process of bioactive agent delivery. This study reports a self-indicating gel fabricated from a cellulose-based derivative, designated as CT, for controlled release of the loaded bioactive agent. By increasing the concentration of CT, the swelling and erosion rates of the gel are significantly reduced, with the encapsulation efficiency and release sustainability of the gel being substantially enhanced. Such changes in delivery performance can be manifested as changes in the intensity of intrinsic luminescence of the gel, enabling the gel to display self-indicating capacity. By using paclitaxel as a model agent, the gel is demonstrated *in vivo* to effectively reduce the systemic toxicity of the administered agent. Along with its excitation wavelength-dependent emission tunability which allows the wavelength of the excitation source to be changed for convenience and need, our gel shows high potential to be exploited as a self-indicating carrier for delivery of bioactive agents.

1. Introduction

Development of a carrier with tunable delivery performance is desired in bioactive agent delivery because it enhances the controllability of the delivery process [[1], [2], [3], [4], [5]]. Among different types of carriers available in the literature, gels attract extensive interest because of their ease of fabrication, high biocompatibility, and their track record of use in pharmaceutical [[6], [7], [8], [9]] and food applications [[10], [11], [12]]. Over the years, various gels with tunable properties have been reported [[13], [14], [15], [16], [17]]. One example is the gel generated from a blend of sodium alginate and carboxymethylcellulose sodium. By changing the mass percentage of sodium alginate in the blend, the release sustainability of the gel has been found to vary. This gel has previously been adopted, along with the technique of microfluidic electrospray, to generate multicompartiment gel beads and fibers for co-delivery of multiple agents, with each of the co-delivered agents being able to be released at a tunable and controlled rate [18,19]. More recently, a composite gel, which consists of poly(trimethylolpropane ethoxylate triacrylate) microspheres embedded into a gel formed from a starch-based bifunctional emulsion stabilizer, has been developed [20]. By altering the composition ratio of the microspheres, the swelling and erosion rates have been successfully tuned [20]. Along with its capacity of being loaded with agents having different degrees of hydrophilicity [20], the gel can potentially be developed into a carrier for delivering both lipophilic and hydrophilic agents.

Despite the advances as mentioned above, the delivery performance of existing gel-based carriers is controlled predominately by manipulating the process of gel preparation. It can hardly be tuned after gel formation. To address this need, this study reports a self-indicating gel which enables reversible transition between the gel state and the solution state. The gel is fabricated from a cellulose-based derivative, named CT, which is a clusteroluminogenic *in situ*-gel forming polymer previously developed by Lai and coworkers for trackable bioactive agent delivery in which the location and formation of the

gel inside a body can be tracked in real time [21]. Although our previous study has demonstrated that by manipulating the molecular weight of CT, gel properties can be changed [21]. Changing the molecular weight of the polymer, however, has to be done at the stage of CT synthesis. This restricts the tunability of the gel in practice. In this study, we report that by altering the concentration of the gel-forming solution, along with the reversibility of state transition experienced by our gel, delivery performance can be manipulated during and after gel formation. Furthermore, due to the clusteroluminogenic property of CT, changes in gel properties and delivery performance can be manifested externally as changes in the intensity of intrinsic luminescence of our gel, enabling the gel to be used as a self-indicating carrier for controlled delivery of bioactive agents.

2. Materials and methods

2.1. Materials

4-dimethylaminopyridine (DMAP), 1-chloro-2,3-epoxypropane, 2-methylpropenoic acid, and various other chemicals were purchased from Sigma-Aldrich (St. Louis, MO, USA). Dulbecco's Modified Eagle's Medium (DMEM; Gibco, Grand Island, USA), penicillin G-streptomycin sulfate (Life Technologies Corporation, USA), and fetal bovine serum (FBS; Hangzhou Sijiqing Biological Engineering Materials Co., Ltd., China) were used as the cell culture medium. Trypsin-EDTA (0.25% trypsin-EDTA) was obtained from Invitrogen (Carlsbad, CA, USA).

2.2. CT synthesis and gel fabrication

CT was synthesized as previously described from modified cellulose (degree of hydroxypropylation = 7–12%; degree of methylation = 28–30%), designated as CE, whose 2% (w/v) aqueous solution exhibited the viscosity of 15 mPa·s at ambient conditions [21]. It was dissolved in anhydrous DMSO to reach a concentration of 1% (w/v). The solution was injected into 25 mL of distilled water for gel formation. The gel was designated as CL. By increasing the concentration of CT in the DMSO solution from 1% (w/v) to 10% (w/v) and following the same procedure for gel fabrication as described above, a gel with a higher CT concentration was generated. It was designated as CH.

2.3. Determination of the encapsulation efficiency (EE)

Methylene blue (MB), lysozyme (LYS), capecitabine (CAP), and paclitaxel (PTX) were adopted as model agents. To form an agent-loaded gel, CL or CH was prepared as described above, but 0.02 g of a model agent was dissolved in 4 mL of the DMSO solution of CT before injection into distilled water. The gel produced was retrieved by centrifugation for 30 min at a relative centrifugal force of 10,000 × g, followed by the removal of the supernatant. The concentration of unloaded MB was determined by ultraviolet–visible (UV–Vis) spectroscopy at λ_{\max} of 665 nm. The amount of unloaded LYS was estimated by using the Bradford reagent (Sigma-Aldrich, Missouri, USA) as previously described [22]. The concentrations of CAP and PTX were quantified by using reverse-phase ultra-high performance liquid chromatography (UPLC), coupled with a triple quadrupole mass spectrometer (UPLC-MS/MS). The EE was calculated using the following equation:

$$EE(\%) = ml/mt \times 100\%$$

where m_l is the mass of the agent successfully loaded into the gel, and m_t is the total mass of the agent added during the agent encapsulation process.

2.4. Determination of the agent release profile

1 g of the lyophilized agent-loaded gel was placed in 10 mL of PBS (pH 7.4) and incubated at 37 °C in a 5% CO₂ atmosphere. At regular time intervals, 1 mL of the release medium was withdrawn and replenished with the same volume of PBS. The amount of MB released was determined by UV–Vis spectroscopy at λ_{\max} of 665 nm. The amount of LYS released was estimated by using the Bradford reagent (Sigma-Aldrich, Missouri, USA) as previously described [22]. The concentrations of PTX and CAP in the release medium were quantified by using UPLC-MS/MS.

2.5. Determination of the protein activity

An LYS-loaded gel was thoroughly crushed in PBS with mortar and pestle. The debris was removed by filtration. The amount of LYS extracted from the gel was determined by using the Bradford reagent (Sigma-Aldrich, Missouri, USA) as previously described [22]. 100 μ L of a solution containing extracted LYS was added to a cuvette, followed by the addition of 1 mL of a 0.01% (w/v) *Micrococcus lysodeikticus* cell suspension. The activity of extracted LYS was determined as previously reported [21].

2.6. Morphological examination

CE, CT, lyophilized CL, and lyophilized CH were sputter-coated with gold. Their morphological features were observed by using a scanning electron microscope (JSM-6380; JEOL, Tokyo, Japan) operated at an accelerating voltage of 10 kV.

2.7. Photoluminescence (PL) characterization

PL and PL excitation (PLE) measurements were performed by using a FLS920P fluorescence spectrometer (Edinburgh Instruments Ltd., Livingston, UK). The PLE spectrum of the DMSO solution of CT was measured at an emission wavelength of 465 nm.

2.8. Spreadability tests

A drop of a DMSO solution of CT with a desired concentration was placed on a glass slide. The solution was spread on the slide using a scraper. The spreadability of the solution was qualitatively determined.

2.9. Rheological measurements

The viscosity of a DMSO solution of CT before and after injection into distilled water was measured using a Brookfield DV-III Ultra programmable rheometer (Brookfield Engineering Laboratories Inc., Middleboro, MA, USA) with spindles (CP-40). Viscosity parameters were determined at different shear rates at ambient conditions. The equilibration time at every shear rate was set to be 15 s. Viscoelastic properties of CL and CH were also studied by determining the storage modulus (G') and loss modulus (G'').

2.10. Determination of the water content (WC) and swelling ratio

A lyophilized gel was weighed and immersed in 100 mL of PBS (pH 7.4). At regular time intervals, the gel was retrieved by centrifugation for 5 min at a relative centrifugal force of $4000 \times g$, followed by the removal of the supernatant. The swelling ratio and WC of the gel were calculated.

2.11. Evaluation of the erosion behavior

The erosion behavior of the gel was examined as previously described [23]. In brief, a known amount of a lyophilized gel was immersed in PBS (pH 7.4) and incubated at 37 °C. At regular time intervals, the gel was retrieved and dried in an oven at 65 °C. The final dry mass of the gel was recorded.

2.12. Cytotoxicity assays

3T3 mouse fibroblasts were cultured in DMEM supplemented with 10% (v/v) FBS, 100 UI mL⁻¹ penicillin, 100 µg mL⁻¹ streptomycin, and 2 mM L-glutamine. The cells were seeded at a density of 5000 cells per well in a 96-well plate, and incubated for 24 h at 37 °C under a humidified atmosphere of 5% CO₂. An appropriate amount of a lyophilized gel was ground in the fresh cell culture medium using mortar and pestle to obtain a suspension with a desired concentration. During the assay, the medium in each well was replaced with 100 µL of the suspension. The 96-well plate was then incubated at 37 °C under a humidified atmosphere of 5% CO₂ for 5 h before the suspension in each well was replaced with the fresh cell culture medium. The percentage of viable cells in each well was evaluated, either immediately or after 24 h of post-treatment incubation, by using the CellTiter 96 Aqueous Non-radioactive Cell Proliferation Assay (MTS assay; Promega Corp., Madison, WI) according to the protocol provided by the manufacturer.

2.13. Evaluation of *in vivo* toxicity

BALB/c nude mice (5 weeks of age, female) were purchased from the Institute of Laboratory Animal Sciences (Beijing, China). BGC-823 xenograft models were established as previously described [21]. All procedures were approved by the Animal Subjects Ethics Sub-committee (ASESC) of the Hong Kong Polytechnic University (approval number: 19-20/118-ABCT-R-STUDENT), and complied with the ARRIVE guidelines and EU Directive 2010/63/EU for animal experiments. When the tumor reached a volume of 100 mm³, the mice were weighed, coded, and randomly divided into 2 groups, with 7 mice in each group. Each mouse was administered intraperitoneally with PTX, at a dose of 20 mg/kg body weight, either in the form of a DMSO solution of PTX or of a PTX-containing CT solution which was prepared as described in Section 2.3. The treatment was performed on day 1, day 4 and day 8. The body weight of the mice was monitored regularly.

2.14. Blood collection and hemolysis assays

Blood was collected from anesthetized BALB/c nude mice (5 weeks of age, female) via cardiac puncture, stored in a heparin-containing tube, and centrifuged at 4 °C for 10 min at 2000 x g to obtain erythrocytes. All procedures were approved by the ASESC of the Hong Kong Polytechnic University (approval number: 19-20/118-ABCT-R-STUDENT), and complied with the ARRIVE guidelines and EU Directive 2010/63/EU for animal experiments. The collected erythrocytes were washed with PBS (pH = 7.4) until the

supernatant became colorless. Procedures for treating the erythrocytes with CT and performing the hemolysis assay were carried out as previously reported [21].

2.15. Statistical analysis

All values were expressed as the mean \pm standard deviation. Unless otherwise specified, the mean value was obtained by averaging five replicates. Student's t-test was carried out to determine the statistical significance. Differences with p-value < 0.05 were considered to be statistically significant. Statistical analysis was performed using GraphPad Prism 8.2.0 software (GraphPad Software Inc., San Diego, CA, USA).

3. Results and discussion

3.1. Synthesis and rheological properties of CT

CT is a cellulose derivative, whose synthesis starts from hydroxypropylation and methylation of cellulose, followed by transesterification which is facilitated by using a polar aprotic solvent as the reaction medium [21]. The DMSO solution of CT has a PL peak at 465 nm and a PLE peak at 380 nm (Fig. 1A); however, the solution shows excitation-dependent emission. Excitation at 340 nm gives an emission peak at 440 nm. When the excitation wavelength is increased to 480 nm, the emission peak is shifted to 560 nm (Fig. 1B). The intrinsic luminescence of CT is attributed to interactions among electron-rich heteroatoms [particularly those from functional groups such as C=O, N=O, and C=N] as sub-fluorophores [24,25]. Such interactions help narrow down the energy gap between the HOMO and LUMO to render CT luminescent despite the absence of a conjugated structure [[26], [27], [28], [29]].

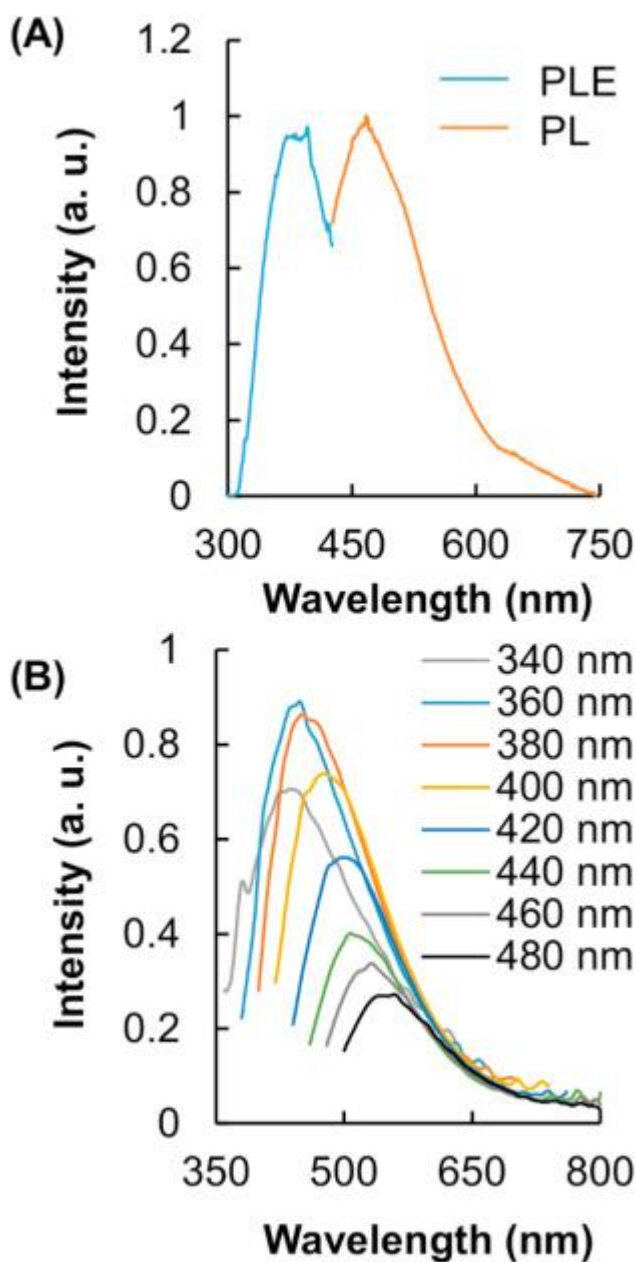


Fig. 1. (A) PLE and PL spectra of the DMSO solution of CT. The PL spectrum was taken at an excitation wavelength of 380 nm; whereas the PLE spectrum was measured at an emission wavelength of 465 nm. (B) PL spectra of the DMSO solution of CT taken at different excitation wavelengths.

After transesterification, the granular morphology of CE is changed to the fibrillar one (Fig. 2A). This is because the incorporated side chains can agglomerate to make the morphology of the product fibril-like [23]. The viscosity of the CT solution, before and after injection into distilled water, at 25 °C is shown in Fig. 2B and C. Compared to that of the 1% (w/v) solution, the spreadability of the 10% (w/v) solution is substantially lower (Fig. 2B). This may be because the viscosity of the 10% (w/v) solution is much higher than that of the 1% (w/v) counterpart. Rheological analysis reveals that the apparent viscosity of the CT

solution, before and after injection into distilled water, is greater at a low shear rate (Fig. 2C). This suggests that pseudoplastic behavior is exhibited by the CT solution and by the fabricated gel. The viscosity of the CT solution is positively related to the CT concentration. This is explained by the fact that an increase in the solution concentration leads to a decrease in the intermolecular distance. The viscosity of the CT solution also increases remarkably after injection into distilled water, owing to the gelation of the solution. Compared to CL, CH has higher G' and G'' values (Fig. 2D). This is explained by the positive relationship between the extent of molecular entanglement and the concentration of the gel-forming solution. An increase in the extent of molecular entanglement can lead to the formation of a gel with enhanced mechanical strength. In addition, in both CL and CH, G' values are higher than G'' values. This implies that both of the gels exhibit solid-like behavior and are robust.

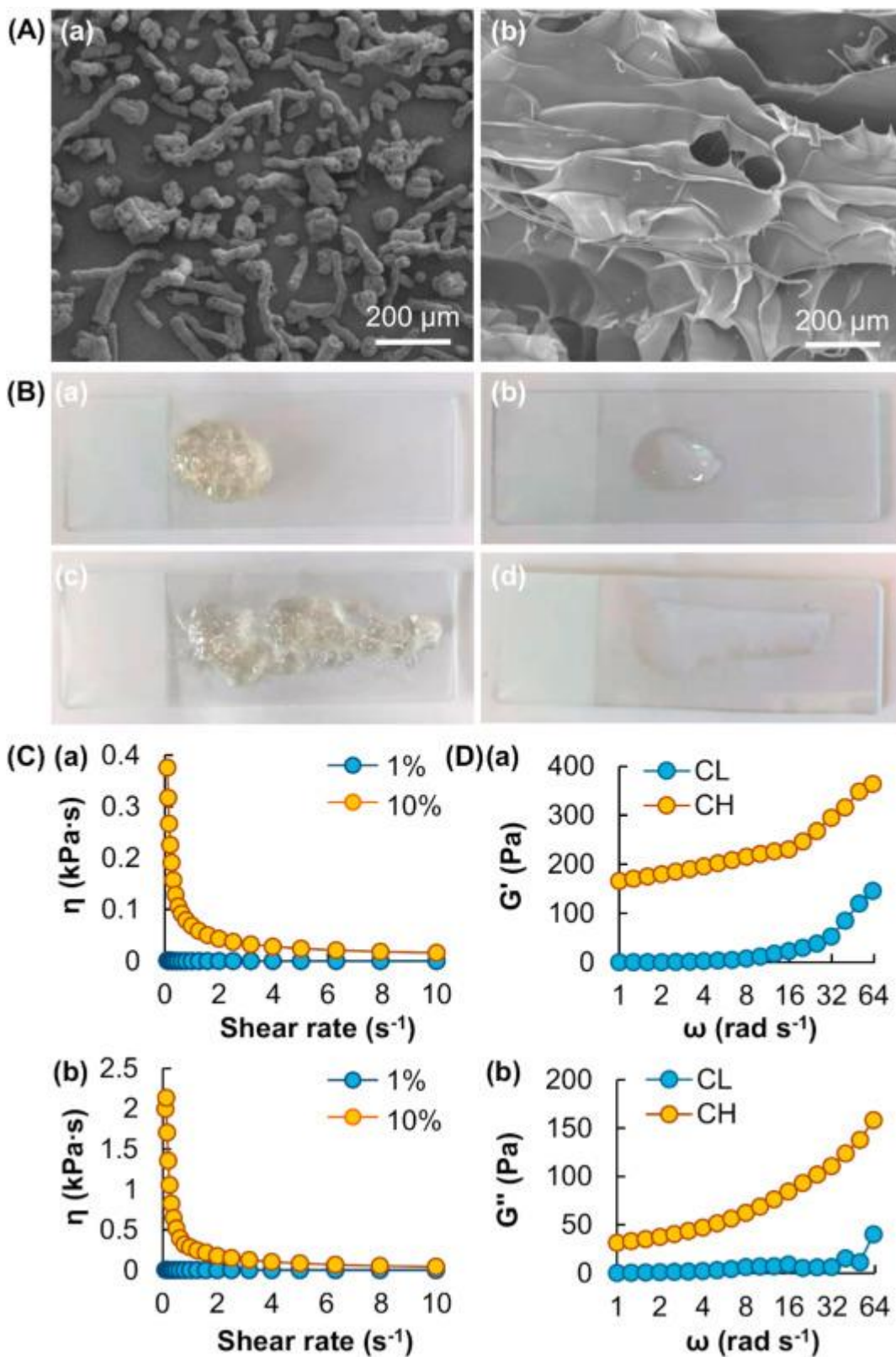


Fig. 2. (A) SEM images of (a) CE and (b) CT. (B) Photos of CT solutions with different concentrations [(a, c) 1% and (b, d) 10%] (a, b) before and (c, d) after spreading. (C) Viscosity curves of CT solutions with different concentrations. Measurements were

made (a) before and (b) after injection of the solutions into distilled water. (D) Changes in (a) G' and (b) G'' values of CL and CH along with changes in the angular frequency.

3.2. Agent encapsulation and bioactivity maintenance

By changing the concentration of the gel-forming solution, the level of entanglement per unit volume of the gel increases, leading to the formation of a gel with a more compact structure. This is confirmed by using scanning electron microscopy (SEM) (Fig. 3A), and explains the fact that, compared to CL, CH displays a remarkably lower swelling ratio, lower WC, and lower erosion susceptibility (Fig. 3B and C). To examine the efficiency of CL and CH in agent encapsulation, MB, LYS, CAP, and PTX are adopted. The EE of the gel varies with various factors (including the concentration of the gel-forming solution, and the solubility and molecular weight of the model agent), and is in the range of 13–94% (Fig. 4A). The optimal EE of the gel formed from CT is comparable to the reported EE (around 60–80%) of formulations or carriers generated from other cellulose derivatives (such as hydroxypropyl methylcellulose [30] or carboxymethyl cellulose [31]).

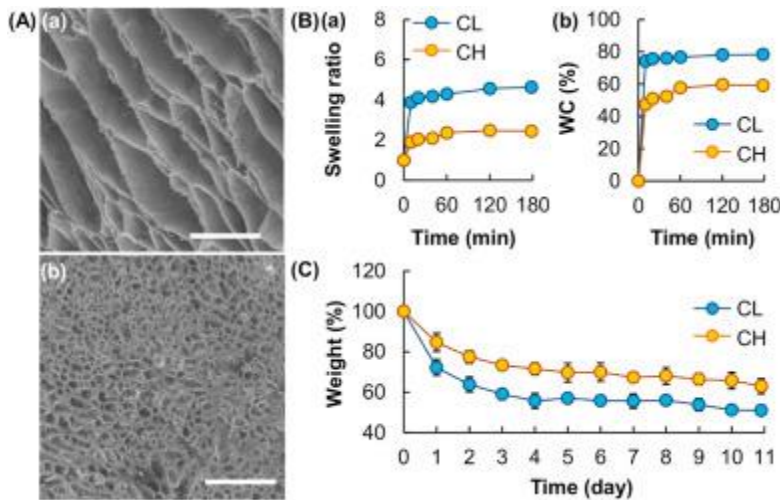


Fig. 3. (A) SEM images of (a) lyophilized CL and (b) lyophilized CH. Scale bar = 500 μm . (B) The swelling capacity of CL and CH as shown by the (a) swelling ratio and (b) WC. (C) Erosion profiles of CL and CH.

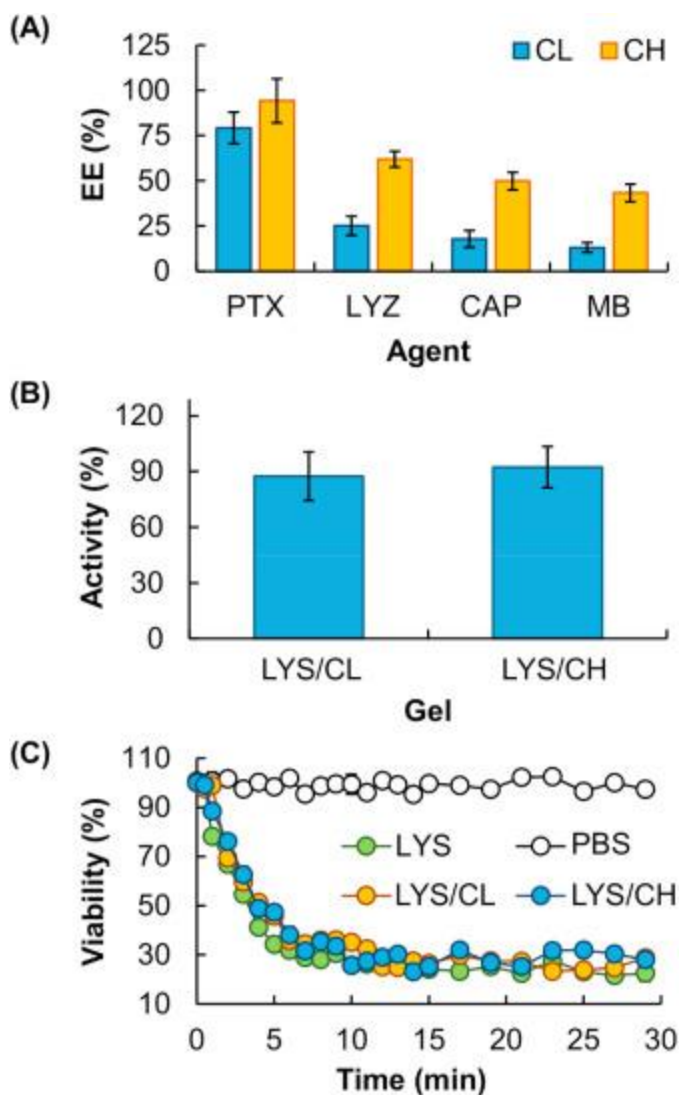


Fig. 4. (A) The EE of CL and CH. (B) The antibacterial activity of LYS extracted from LYS-loaded CL (LYS/CL) and LYS-loaded CH (LYS/CH). The activity of pure LYS is taken as 100%. (C) Time-dependent changes in the viability of *Micrococcus lysodeikticus* after addition of LYS extracted from LYS/CL and LYS/CH. The LYS solution and PBS were used as the controls.

In order to be used practically as a carrier of bioactive agents, not only should the gel possess high EE but it should also maintain the bioactivity of the loaded agents [32,33]. Unlike photopolymerized gels in which exposure of the loaded agents to UV may compromise the agent stability [[34], [35], [36]], gelation of CT takes place under mild conditions without having a need for UV irradiation or any other physical/chemical initiators, thereby enabling CL and CH to more effectively maintain the bioactivity of the loaded agent. This is evidenced by the high antibacterial activity level (over 80%) of LYS extracted from the LYS-loaded gels (*viz.*, LYS/CL and LYS/CH), as revealed by the high rate of lysis of *Micrococcus lysodeikticus* (Fig. 4B and C). This suggests that the antibacterial activity of LYS is not affected by the gel fabrication process or by possible interactions between the gel components and the protein.

3.3. Biocompatibility and tunable agent release

The intensity of blue emission of the CT solution, as well as that of the gel formed, is positively related to the CT concentration (Fig. 5A–C), which also has a positive relationship with the release sustainability of the gel (Fig. 5D). This enables the gel to possess self-indicating properties, by which the delivery performance of an agent-loaded gel can be estimated even before use. The working principle is that by increasing the concentration of CT, the extent of molecular entanglement (and hence clusterization-triggered emission) is enhanced [21]. Meanwhile, agent release from a matrix-type device is generally driven by Fickian diffusion, which is partly governed by the degree of swelling exhibited by the device [37]. Changes in the concentration of CT directly affect the swelling and erosion rates of the gel, leading to changes in release sustainability. The concentration of CT, therefore, serves as a bridging factor between release sustainability and the luminescence intensity, allowing the possible use of the luminescence of CT as an indicator to predict the delivery performance of the gel.

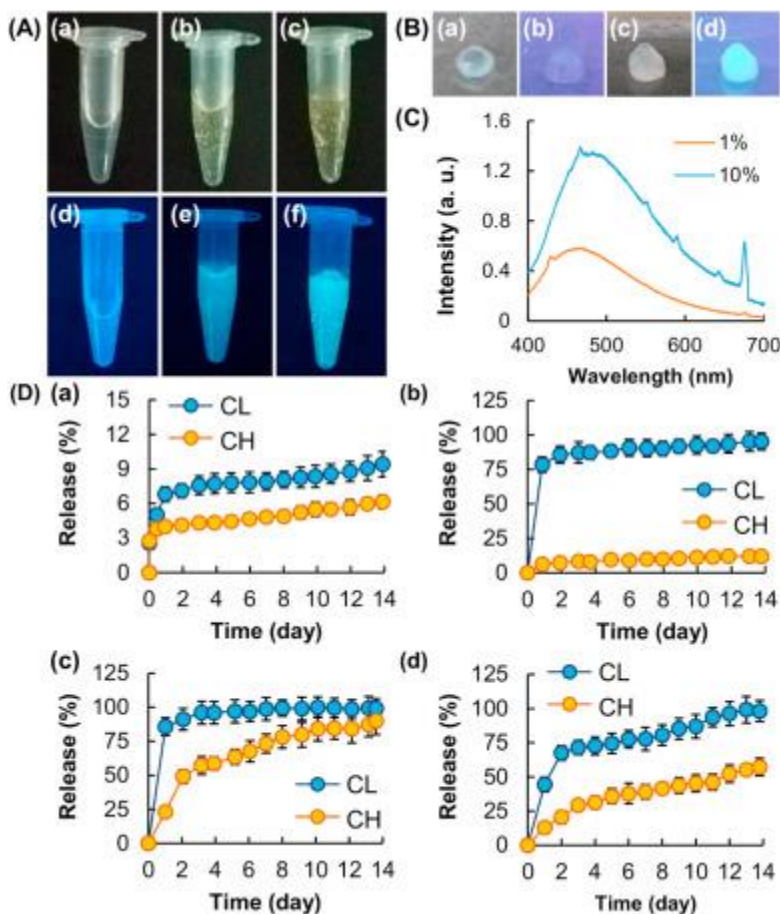


Fig. 5. (A) Photos of CT solutions with different concentrations [(a, d) 1%, (b, e) 5%, and (c, f) 10%] under (a–c) visible light and (d–f) UV light. (B) Photos of (a, b) CL and (c, d) CH under (a, c) visible light and (b, d) UV light. (C) PL spectra of CT solutions with different concentrations. The spectra were taken at an excitation wavelength of 380 nm. (D) Release profiles of (a) PTX, (b) CAP, (c) MB, and (d) LYS from agent-loaded CL and agent-loaded CH.

The tunability of the gel performance is mediated by the fact that the CT solution can switch to the gel state upon injection into water, with the gel being able to get back to the solution state upon the addition of DMSO (Fig. 6A). To demonstrate that state transition has no effect on the delivery performance of the gel, the release profile of LYS from LYS/CL and LYS/CH, with or without undergoing one cycle of state transition (from the gel state to the solution state, and finally back to the gel state), is determined. Results show that the effect of state transition on the release rate of the loaded agent from both CL and CH is negligible (Fig. 6B). This suggests that whenever the performance of a pre-formed gel has to be changed, one can simply convert the gel back to the solution state, followed by adjustment of the CT concentration to the desired level before re-gelation of the solution. Contrary to many existing gel-based systems whose delivery performance is controlled predominately by manipulating conditions during gel preparation and hence *post-hoc* tuning of the gel performance is difficult, the delivery performance of CL and CH can be easily tuned in a *post-hoc* manner.

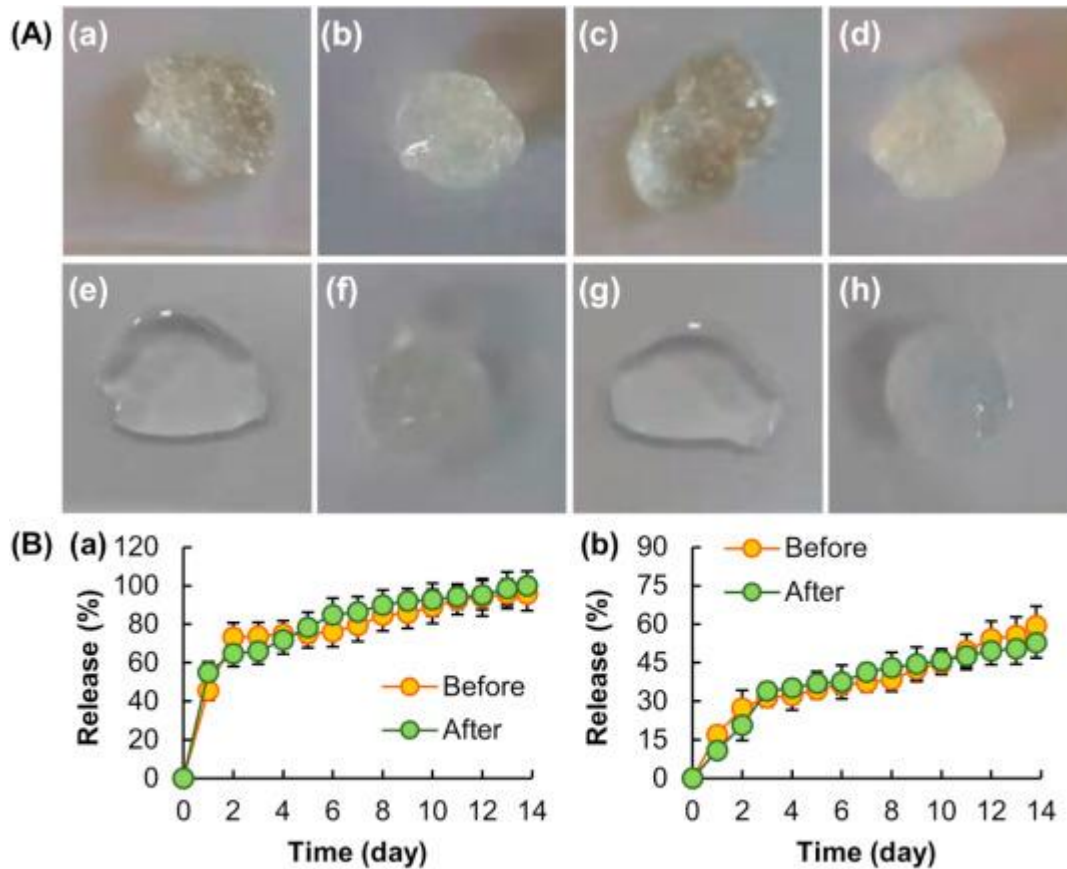


Fig. 6. (A) Reversible state transition experienced by CT solutions with different concentrations [(a–d) 10%, and (e–h) 1%]. (a, e) CT solutions switch to the (b, f) gel state upon injection into distilled water. (c, g) The gels are converted back to the solution state upon the addition of DMSO. (d, h) The solutions formed undergo re-gelation upon injection into distilled water. (B) Release profiles of LYS from (a) agent-loaded CL and (b) agent-loaded CH, before and after one cycle of state transition. Finally, the toxicity of CT is assessed by using 3T3 fibroblasts as a model system. Results show that the toxicity of CT is negligible (Fig. 7A). The negligible hemolytic

activity exhibited by CT also demonstrates the high biocompatibility of the polymer (Fig. 7B). The safety profile of CT is determined *in vivo* by using PTX as a model bioactive agent. From day 2 onwards, the relative body weight of mice treated with a DMSO solution of PTX is significantly lower than that of mice in the PTX/CT group (Fig. 7C). This is attributed to the fact that the gel formed from CT can lead to sustained release of PTX. This reduces the systemic drug concentration, resulting in a decline in the systemic toxicity brought about by PTX.

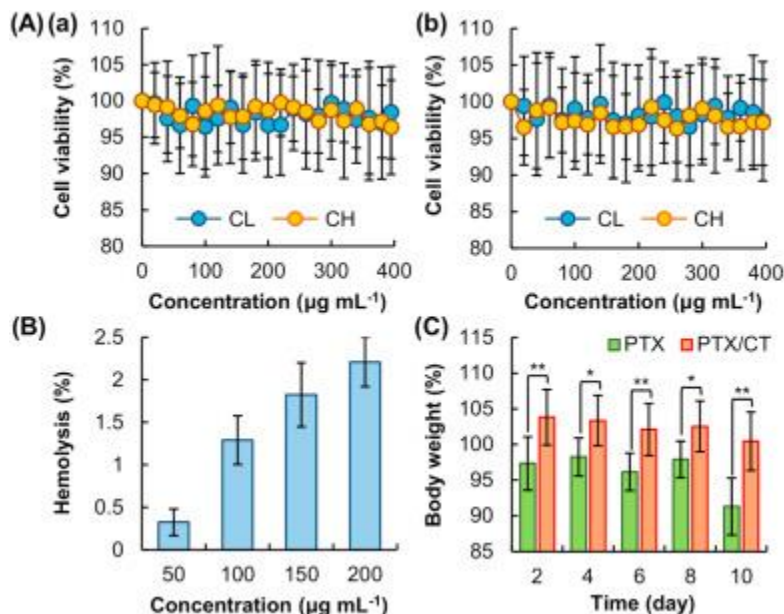


Fig. 7. (A) Viability of 3T3 fibroblasts after 5-h treatment with different concentrations of CL or CH, (a) before and (b) after 24-h post-treatment incubation. (B) Percentages of erythrocytes lysed upon treatment with different concentrations of CT. (C) Changes in the relative body weight of mice injected intraperitoneally with either a DMSO solution of PTX or a PTX-containing DMSO solution of CT. * denotes $p < 0.05$ and ** denotes $p < 0.01$.

4. Conclusions

So far the tuning of the delivery performance of existing gel-based carriers has been relying largely on the manipulation of the process of gel preparation. This restricts the possibility of changing the gel performance in a *post-hoc* manner. This study reports a self-indicating gel which not only shows tunable efficiency in delivering bioactive agents, but also displays intrinsic luminescence whose intensity can serve as an indicator revealing the delivery performance of the gel even before use. In addition, due to the excitation wavelength-dependent emission tunability, the wavelength of the excitation source can be chosen on the basis of convenience and need. This, along with its low toxicity and high biocompatibility as demonstrated both *in vitro* and *in vivo*, the gel formed from CT has high potential to be exploited as a tunable carrier for use in bioactive agent delivery in the future.

Credit author statement

W. F. Lai: Conceptualization, Funding acquisition, Investigation, Project administration, Resources, Supervision, Validation, Writing - original draft, Writing - review & editing. **D. Gui:** Resources. **M. G. Wong:** Investigation. **A. Döring:** Investigation. **A. L. Rogach:** Resources, Writing - review & editing. **T. He:** Resources. **W. T. Wong:** Resources, Funding acquisition, Validation.

Declaration of competing interest

The authors declare that they have no conflict of interest.

Acknowledgements

This work was supported by the Chinese University of Hong Kong, Shenzhen (PF01001421, UDF01001421 and UF02001421) and the Research Grants Council of the Government of Hong Kong Special Administrative Region (C5012-15E and CityU 11306619).

References

- [1] A. Roy, S. Jhunjhunwala, E. Bayer, M. Fedorchak, S.R. Little, P.N. Kumta, Porous calcium phosphate-poly (lactic-co-glycolic) acid composite bone cement: a viable tunable drug delivery system, *Mater. Sci. Eng. C Mater. Biol. Appl.* 59 (2016) 92–101.
- [2] P. Tipduangta, P. Belton, L. Fabian, L.Y. Wang, H. Tang, M. Eddleston, S. Qi, Electrospun polymer blend nanofibers for tunable drug delivery: the role of transformative phase separation on controlling the release rate, *Mol. Pharm.* 13 (1) (2016) 25–39.
- [3] E. Mauri, F. Rossi, A. Sacchetti, Tunable drug delivery using chemoselective functionalization of hydrogels, *Mater. Sci. Eng. C Mater. Biol. Appl.* 61 (2016) 851–857.
- [4] A. Al Samad, A. Bethry, E. Koziolova, M. Netopilik, T. Etrych, Y. Bakkour, J. Coudane, F. El Omar, B. Nottelet, PCL-PEG graft copolymers with tunable amphiphilicity as efficient drug delivery systems, *J. Mater. Chem. B* 4 (37) (2016) 6228–6239.
- [5] Y. Li, N. Li, W. Pan, Z. Yu, L. Yang, B. Tang, Hollow mesoporous silica nanoparticles with tunable structures for controlled drug delivery, *ACS Appl. Mater. Interfaces* 9 (3) (2017) 2123–2129.
- [6] L.M. Suta, A. Tudor, C.R. Sandulovici, L. Stelea, D. Hadaruga, C. Mircioiu, G. S. Balint, Multivariate statistical analysis regarding the formulation of oxcam-based pharmaceutical hydrogels, *Rev. Chim.* 68 (4) (2017) 726–731.
- [7] R. Lopez-Cebral, P. Paolicelli, V. Romero-Caamano, B. Seijo, M.A. Casadei, A. Sanchez, Spermidine-cross-linked hydrogels as novel potential platforms for pharmaceutical applications, *J. Pharm. Sci.* 102 (8) (2013) 2632–2643.
- [8] W. Farhat, R. Venditti, N. Mignard, M. Taha, F. Becquart, A. Ayoub, Polysaccharides and lignin based hydrogels with potential pharmaceutical use as a drug delivery system produced by a reactive extrusion process, *Int. J. Biol. Macromol.* 104 (2017) 564–575.
- [9] C.S.A. de Lima, T.S. Balogh, J.P.R.O. Varca, G.H.C. Varca, A.B. Lugao, L. A. Camacho-Cruz, E. Bucio, S.S. Kadlubowski, An updated review of macro, micro, and nanostructured hydrogels for biomedical and pharmaceutical applications, *Pharmaceutics* 12 (10) (2020) 970.
- [10] L.S. Liu, J. Kost, F. Yan, R.C. Spiro, Hydrogels from biopolymer hybrid for biomedical, food, and functional food applications, *Polymers* 4 (2) (2012) 997–1011.

- [11] M.S. Lindblad, A.C. Albertsson, New materials based on hemicelluloses: hydrogels and food delivery materials, *Abstr. Pap. Am. Chem. Soc.* 227 (2004) U282–U283.
- [12] S. Farris, K.M. Schaich, L.S. Liu, L. Piergiovanni, K.L. Yam, Development of polyion-complex hydrogels as an alternative approach for the production of bio-based polymers for food packaging applications: a review, *Trends Food Sci. Technol.* 20 (8) (2009) 316–332.
- [13] B. Stella, I. Andreana, D. Zonari, S. Arpicco, Pentamidine-loaded lipid and polymer nanocarriers as tunable anticancer drug delivery systems, *J. Pharm. Sci.* 109 (3) (2020) 1297–1302.
- [14] A. Passi, D. Vigetti, Hyaluronan as tunable drug delivery system, *Adv. Drug Deliv. Rev.* 146 (2019) 83–96.
- [15] W.F. Lai, C. Hu, G. Deng, K.H. Lui, X. Wang, T.H. Tsoi, S. Wang, W.T. Wong, A biocompatible and easy-to-make polyelectrolyte dressing with tunable drug delivery properties for wound care, *Int. J. Pharm.* 566 (2019) 101–110.
- [16] R.C.F. Goncalves Lopes, O.F. Silvestre, A.R. Faria, C.d.V. Ml, E.F. Marques, J. B. Nieder, Surface charge tunable cationic vesicles based on serine-derived surfactants as efficient nanocarriers for the delivery of the anticancer drug doxorubicin, *Nanoscale* 11 (13) (2019) 5932–5941.
- [17] S.R. Abulatefeh, M.Y. Alkawareek, A.M. Alkilany, Tunable sustained release drug delivery system based on mononuclear aqueous core-polymer shell microcapsules, *Int. J. Pharm.* 558 (2019) 291–298.
- [18] W.F. Lai, A.S. Sussha, A.L. Rogach, Multicompartment microgel beads for co-delivery of multiple drugs at individual release rates, *ACS Appl. Mater. Interfaces* 8 (1) (2016) 871–880.
- [19] W.F. Lai, E. Huang, K.H. Lui, Alginate-based complex fibers with the Janus morphology for controlled release of co-delivered drugs, *Asian J. Pharm. Sci.* (2020), <https://doi.org/10.1016/j.ajps.2020.05.003>.
- [20] W.F. Lai, A.L. Rogach, W.T. Wong, One-pot synthesis of an emulsion-templated hydrogel-microsphere composite with tunable properties, *Compos. Part A-Appl. S.* 113 (2018) 318–329.
- [21] W.F. Lai, E. Huang, W.T. Wong, A gel-forming clusteroluminogenic polymer with tunable emission behavior as a sustained-release carrier enabling real-time tracking during bioactive agent delivery, *Appl. Mater. Today* 21 (2020) 100876.
- [22] W.F. Lai, H.C. Shum, A stimuli-responsive nanoparticulate system using poly(ethylenimine)-graft-polysorbate for controlled protein release, *Nanoscale* 8(1) 517–528.
- [23] W.F. Lai, H.C. Shum, Hypromellose-graft-chitosan and its polyelectrolyte complex as novel systems for sustained drug delivery, *ACS Appl. Mater. Interfaces* 7(19) 10501–10510.
- [24] L. Viglianti, N.L.C. Leung, N. Xie, X.G. Gu, H.H.Y. Sung, Q. Miao, I.D. Williams, E. Licandro, B.Z. Tang, Aggregation-induced emission: mechanistic study of the clusteroluminescence of tetrathienylethene, *Chem. Sci.* 8 (4) (2017) 2629–2639.
- [25] W.F. Lai, Non-conjugated polymers with intrinsic luminescence for drug delivery, *J. Drug Deliv. Sci. Technol.* 59 (2020) 101916.
- [26] R. Hoffmann, Interaction of orbitals through space and through bonds, *Acc. Chem. Res.* 4 (1) (1971) 1–9.

- [27] X.G. Guo, J. Quinn, Z.H. Chen, H. Usta, Y. Zheng, Y. Xia, J.W. Hennek, R.P. Ortiz, T.J. Marks, A. Facchetti, Dialkoxybithiazole: a new building block for head-to-head polymer semiconductors, *J. Am. Chem. Soc.* 135 (5) (2013) 1986–1996.
- [28] N. Hergue, C. Mallet, G. Savitha, M. Allain, P. Frere, J. Roncali, Facile synthesis of 3-alkoxy-4-cyanothiophenes as new building blocks for donor-acceptor conjugated systems, *Org. Lett.* 13 (7) (2011) 1762–1765.
- [29] A.S. Ozen, C. Atilgan, G. Sonmez, Noncovalent intramolecular interactions in the monomers and oligomers of the acceptor and donor type of low band gap conducting polymers, *J. Phys. Chem. C* 111 (44) (2007) 16362–16371.
- [30] I.S.M. Zaidul, T.K. Fahim, F. Sahena, A.K. Azad, M.A. Rashid, M.S. Hossain, Dataset on applying HPMC polymer to improve encapsulation efficiency and stability of the fish oil: in vitro evaluation, *Data Brief* 32 (2020) 106111.
- [31] W.F. Lai, A.S. Susha, A.L. Rogach, G.A. Wang, M.J. Huang, W.J. Hu, W.T. Wong, Electrospray-mediated preparation of compositionally homogeneous core-shell hydrogel microspheres for sustained drug release, *RSC Adv.* 7 (70) (2017) 44482–44491.
- [32] W.F. Lai, A.L. Rogach, Hydrogel-based materials for delivery of herbal medicines, *ACS Appl. Mater. Interfaces* 9 (13) (2017) 11309–11320.
- [33] W.F. Lai, Z.D. He, Design and fabrication of hydrogel-based nanoparticulate systems for in vivo drug delivery, *J. Contr. Release* 243 (2016) 269–282.
- [34] Y.Q. Zhang, J.F. Zhang, Y.J. Xiao, V.W.C. Chang, T.T. Lim, Direct and indirect photodegradation pathways of cytostatic drugs under UV germicidal irradiation: process kinetics and influences of water matrix species and oxidant dosing, *J. Hazard Mater.* 324 (2017) 481–488.
- [35] M. Litvic, K. Smic, V. Vinkovic, M. Filipan-Litvic, A study of photodegradation of drug rosuvastatin calcium in solid state and solution under UV and visible light irradiation: the influence of certain dyes as efficient stabilizers, *J. Photochem. Photobiol., A* 252 (2013) 84–92.
- [36] S. Sijak, N. Liu, M. Zheng, G. Xu, L. Tang, J.Z. Yao, M.H. Wu, Degradation of anticonvulsant drug primidone in aqueous solution by UV photooxidation processes, *Environ. Eng. Sci.* 32 (5) (2015) 436–444.
- [37] J. Siepmann, F. Siepmann, Mathematical modeling of drug delivery, *Int. J. Pharm.* 364 (2) (2008) 328–343.